SUPPLEMENT FIGURE LEGENDS

Supplement Figure 1.

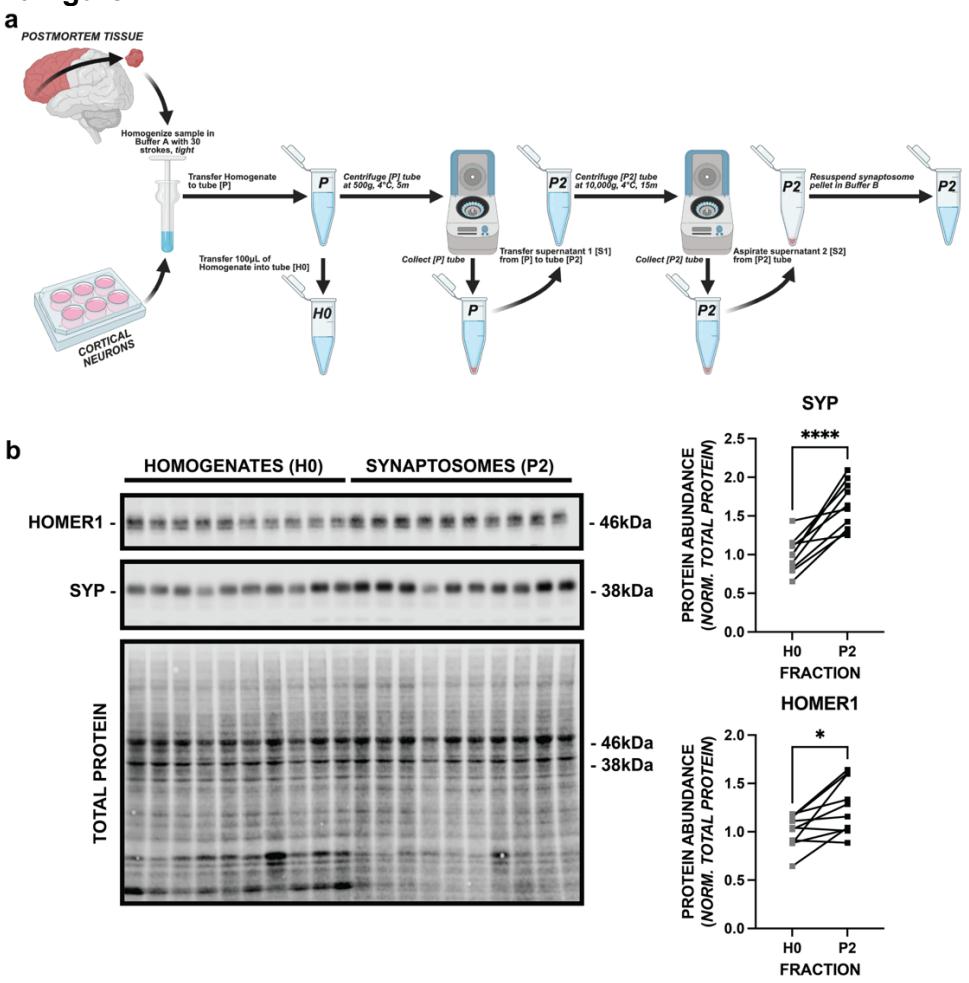

Supplement Figure 1. Biochemical fractionation and enrichment of frontal cortex synaptosomes.

a: Biochemical fractionation of synaptosomes: Schematic diagram illustrating the workflow of synaptosome isolation, in both frontal cortex and iPSC-cortical neuron models, where the sample is homogenized (H0 fraction) and subjected to a series of differential centrifugation to derive the synaptosome fraction (P2) (centrifuged at 500xg to separate cytosol from cell debris, and the supernatant 1 (S1) centrifuged at 10,000xg to separate the cytosol from the crude synaptosome pellet).

b: Western Blot Validation: Synaptic protein enrichment across homogenate (H0) and synaptosome (P2) fractions. Western blot quantification shows enrichment of presynaptic *Synaptophysin* in the P2 fraction (Welch's t-test, $p<0.0001$), and enrichment of postsynaptic *Homer1* in the P2 fraction (Welch's t-test, $p<0.05$), both normalized to total protein abundance.

Supplement Figure 2.

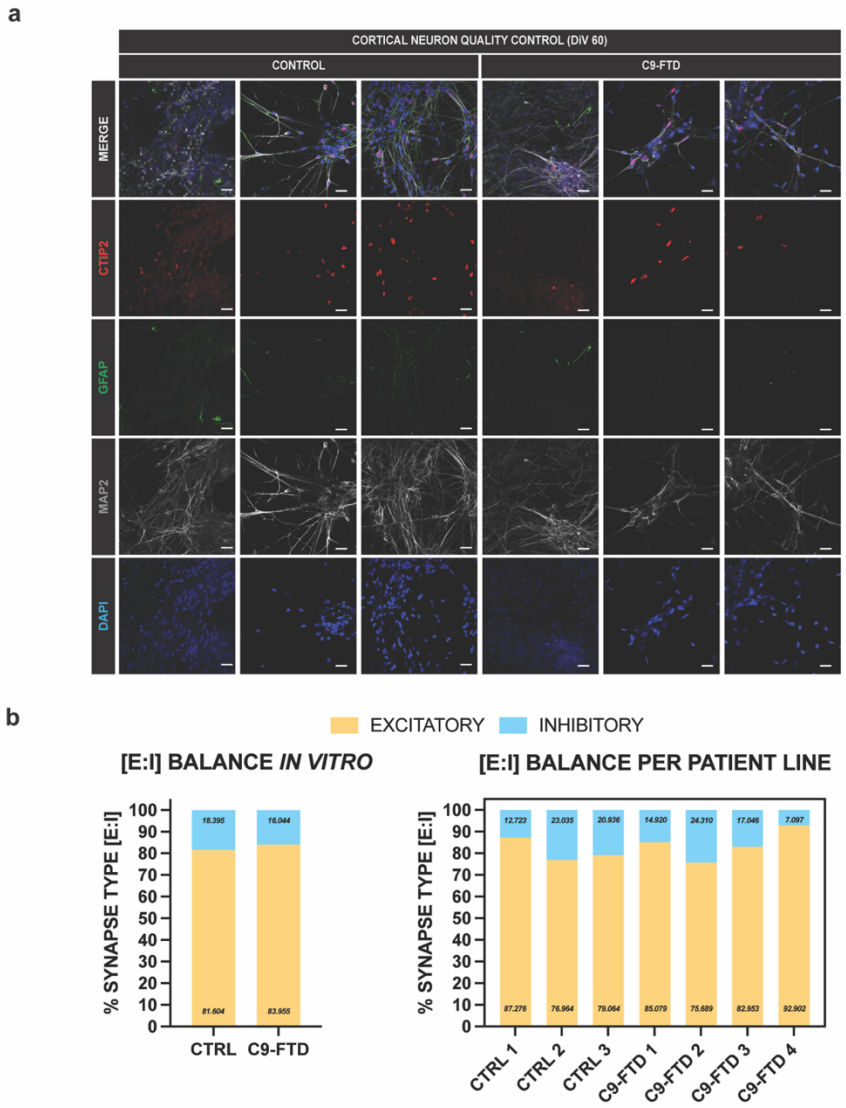

Supplement Figure 2. Generation of iPSC-Cortical Neurons and Excitatory-to-Inhibitory synapse composition.

a: Cortical neuron marker expression: Representative immunofluorescence images from three control and three C9-FTD of patient-derived iPSC-cortical neurons used in this study at DiV 60 for marker, *CTIP2,* neuronal marker *MAP2*, and astrocytic *GFAP*. Immunofluorescence analysis confirming the high presence of cortical neuron markers and limited astrocytic contamination. *Scale bar=20μM.*

b: Excitatory-Inhibitory synapse balance: Quantification of excitatory and inhibitory synaptic puncta in DiV 100 control and C9-FTD iPSC-cortical neuron cultures. Excitatory synapses were identified by the colocalization of VGLUT1 and Homer1, and inhibitory synapses identified by the colocalization of VGAT and Gephyrin. The proportion of each synapse type was calculated as the number of excitatory or inhibitory puncta divided by the sum of total colocalized synaptic puncta. Summary data are shown as a stacked bar graph representing the percentage of excitatory and inhibitory synapses across control and C9-FTD cultures (left). Individual cell-line distributions (right) demonstrate the E:I neuronal proportions across control and C9-FTD lines. Cortical neurons were differentiated using dual-SMAD inhibition to generate forebrain, excitatory neurons [Shi et al 2012].

Supplement Figure 3.

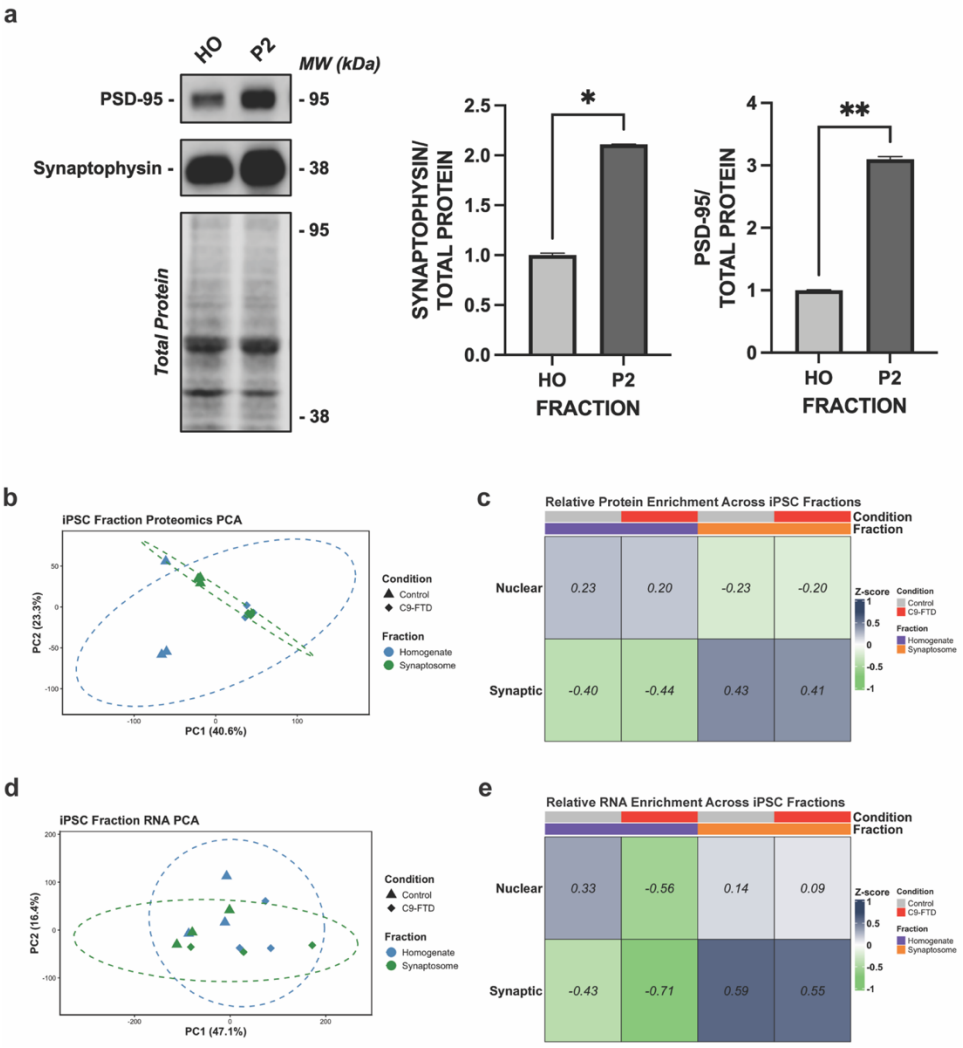

Supplement Figure 3. Successful synaptosome enrichment in iPSC-cortical neuron models.

a: Western Blot Validation: Synaptic protein enrichment across homogenate (H0) and synaptosome (P2) fractions. Western blot quantification shows enrichment of presynaptic *Synaptophysin* in the P2 fraction (Welch's t-test, $p<0.05$; ± SEM), and enrichment of postsynaptic *PSD-95* in the P2 fraction (Welch's t-test, $p<0.05$; ± SEM), both normalized to total protein abundance.

b: Distinct Molecular Profiles by Fraction: Principal Component Analysis (PCA) of proteomic data from homogenate (H0) and synaptosome (P2) fractions across control and C9-FTD iPSC-cortical neurons (PCA1=40.6%, PC2=23.3%), demonstrating sample separation by disease status and biochemical fraction identity.

c: Compartmental Enrichment of Synaptic Signatures: Z-score-normalized heatmap of synaptic protein abundance across H0 and P2 fractions in control and C9-FTD iPSC-cortical neurons, highlighting enrichment of synaptic gene sets in the P2 fraction and nuclear gene set enrichment in the H0 fraction.

d: Distinct Molecular Profiles by Fraction: PCA of transcriptomic data from iPSC-cortical neuron-derived H0 and P2 fractions (PC1=47.1%, PC2=16.4%), demonstrating sample separation by disease status and biochemical fraction identity.
e: Compartmental Enrichment of Synaptic Signatures: Z-score-normalized heatmap of synaptic RNA abundance across H0 and P2 fractions, highlighting enrichment of synaptic gene sets in the P2 fraction.

Supplement Figure 4

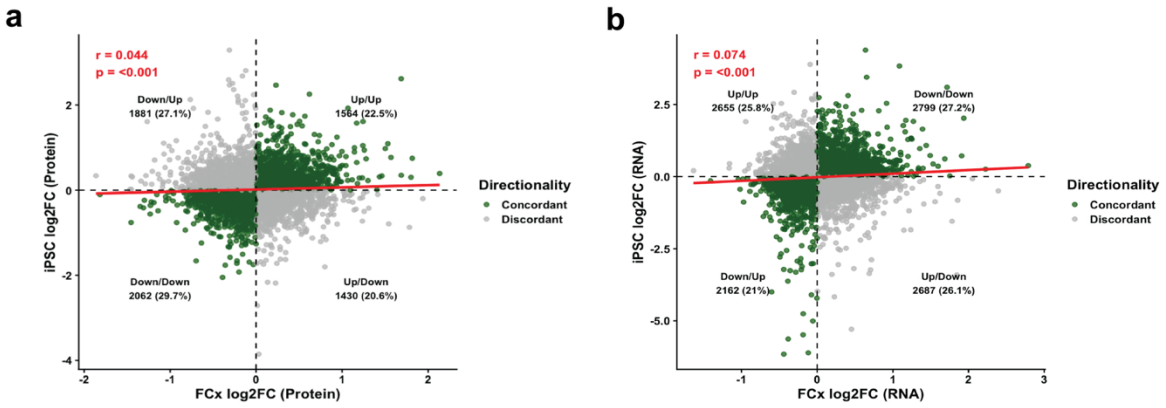

Supplement Figure 4. Correlation of protein and RNA expression across frontal cortex and iPSC-derived synaptosomes.

a: Protein Concordance across Frontal Cortex and iPSCs: Correlation analysis of frontal cortex synaptic proteome (x-axis) and iPSC synaptosome proteome (y-axis) log_2FC. The correlation was modest (Pearson r=0.044, p<0.001), however a substantial proportion of proteins exhibited concordant regulation across model systems, with 22.5% of proteins concordantly upregulated and 29.7% of proteins concordantly downregulated. The presence of discordant proteins (grey) highlights specific differences between frontal cortex and iPSC-derived synaptic proteomes.

b: Transcriptional Concordance across Frontal Cortex and iPSCs: Correlation analysis of frontal cortex synaptosomal transcriptome (x-axis) and iPSC synapse transcriptome (y-axis) log_2FC. The correlation was modest (Pearson r=0.074, p<0.001) and exceeded proteomic observations. 27.2% of transcripts were concordantly upregulated and 21% of transcripts were concordantly downregulated across model systems, with the presence of discordant transcripts (grey) between models. These changes reflect shared and model-specific aberrations.

Supplement Figure 5

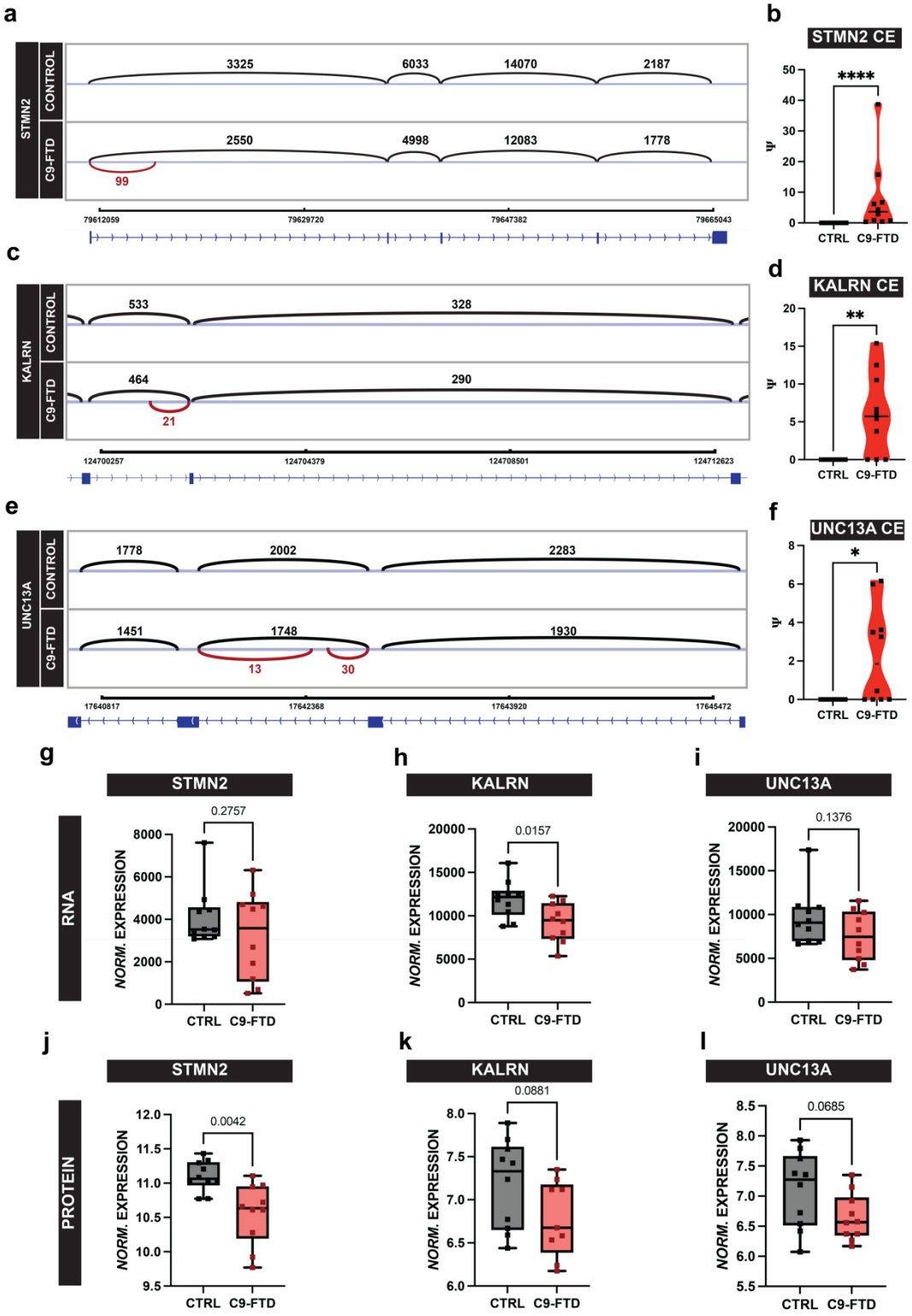

Supplement Figure 5. Alternative Splicing analysis reveals cryptic exon inclusion in C9-FTD frontal cortex homogenates.

a: Detection of STMN2 cryptic exon-containing transcripts: IGV sashimi plot of full-length *STMN2* gene transcripts containing cryptic exon (CE) inclusions. The top track shows the data from combined FCx control cases (n=10). The bottom track shows the data from combined FCx C9-FTD cases (n=10).
b: Detection of Cryptic Exon inclusion: Violin plot displaying the percentage spliced in (PSI) values of CE inclusion in *STMN2* within control and C9-FTD FCx homogenates **(**p<0.0001; Mann-Whitney test test). *Each dot represents each case subject used in this study.*
c: Detection of KALRN cryptic exon-containing transcripts: IGV sashimi plot of full-length *KALRN* gene transcripts containing cryptic exon (CE) inclusions. The top track shows the data from combined FCx control cases (n=10). The bottom track shows the data from combined FCx C9-FTD cases (n=10).
d: Quantification of Cryptic Exon inclusion: Violin plot displaying the PSI values of CE inclusion in *KALRN* within control and C9-FTD FCx homogenates (p=0.0031; Mann-Whitney test). *Each dot represents each case subject used in this study*.
e: Detection of UNC13A cryptic exon-containing transcripts: IGV sashimi plot of full-length *UNC13A* gene transcripts containing cryptic exon (CE) inclusions. The top track shows the data from combined FCx control cases (n=10). The bottom track shows the data from combined FCx C9-FTD cases (n=10).
f: Quantification of Cryptic Exon inclusion: Violin plot displaying the PSI values of CE inclusion in *UNC13A* within control and C9-FTD FCx homogenates (p=0.0108; Mann-Whitney test). *Each dot represents each case subject used in this study.*
g-i: Comparison of normalized gene expression for CE-containing genes in FCx homogenates. *Each dot represents each case subject used in this study.*
g: Box plot displaying normalized gene expression of *STMN2* (p=0.2757; Welch's t-test; ± SEM).
h: Box plot displaying normalized gene expression of *KALRN* (p=0.0157; Welch's t-test; ± SEM).
i: Box plot displaying normalized gene expression of *UNC13A* (p=0.1376; Welch's t-test; ± SEM).
j-l: Comparison of normalized protein expression for CE-containing genes in FCx homogenates. *Each dot represents each case subject used in this study.*
j: Box plot displaying normalized protein expression of *STMN2* (p=0.0042; Welch's t-test; ± SEM).
k: Box plot displaying normalized protein expression of *KALRN* (p=0.0881; Welch's t-test; ± SEM).
l: Box plot displaying normalized protein expression of *UNC13A* (p=0.0685; Welch's t-test; ± SEM).